Nonlinear Harmonic Generation in Free-Electron Lasers with Helical Wigglers

H. P. Freund,[1] P. G. O'Shea,[2] and S. G. Biedron[3]
[1]*Science Applications International Corporation, McLean, VA 22102, USA*
[2]*University of Maryland, College Park, MD 20742, USA*
[3]*Energy Systems Division, Argonne National Laboratory, Argonne, IL 60439, USA*
(Received 2 August 2004; published 25 February 2005)

It is widely believed that harmonics are suppressed in helical wigglers. However, linear harmonic generation (LHG) occurs by an azimuthal resonance that excites circularly polarized, off-axis waves, where the hth harmonic varies as $\exp(ih\theta)$. Nonlinear harmonic generation (NHG) is driven by bunching at the fundamental and has different properites from LHG. While NHG has been studied in planar wigglers, there has been no analysis of NHG in helical wigglers. The 3D simulation code MEDUSA has been modified for this purpose, and it is shown that NHG is substantial in helical wigglers and that the even and odd harmonics have comparable intensities.

DOI: 10.1103/PhysRevLett.94.074802 PACS numbers: 41.60.Cr, 52.59.Rz

It is widely believed that on-axis harmonic generation is weak or suppressed in free-electron lasers (FELs) with helical wigglers [1,2]. Harmonic generation occurs in both planar and helical wigglers, albeit by different mechanisms with different harmonic emission properties. Coherent harmonic generation arises due to linear instabilities, nonlinear bunching, or a combination of the two. Kincaid [1] showed that spontaneous generation from helical wigglers vanishes on axis, and Elias *et al.* [2] failed to observe harmonic emission from a low-gain, helical wiggler FEL amplifier that did not reach saturation. In this Letter, we show that when the fundamental reaches sufficiently high intensities, then nonlinear harmonic generation (NHG) produces high intensities on axis.

There are two principal development paths in FELs at the present time. One path is the development of x-ray light sources using self-amplified spontaneous emission (SASE), where NHG is a benefit since it produces shorter wavelengths with no increase in beam energy. SASE FELs will initially use planar wigglers; however, future light sources may contain helical wiggler beam lines to produce polarized photons, and understanding NHG in helical wigglers is important. The second path is directed at high average power FEL oscillators, where harmonics in the ultraviolet may damage mirror coatings. Hence, NHG is an unwanted side effect. It has been suggested that the use of helical wigglers eliminates the harmonic mirror damage problem. For this reason, we are primarily concerned with NHG in helical wiggler oscillators; however, the results have clear implications for NHG in helical wiggler beam lines in x-ray light sources as well.

Linear harmonic generation (LHG) in planar wigglers arises from linear instabilities due to even harmonic components in the axial velocity that excite linearly polarized, on-axis modes [3–5]. This harmonic motion scales as $(K/\gamma_b)^h$, where h is the harmonic number, K is the wiggler strength parameter, and γ_b is the relativistic factor. Therefore, the harmonic interaction is sensitive to the wiggler strength. Further, while even harmonics can be generated by off-axis wiggler components, the odd harmonics typically have much higher intensities. In contrast, the axial velocity is nearly constant in helical wigglers, and LHG is due to an azimuthal resonance that excites circularly polarized waves [3]. The azimuthal electron motion in helical wigglers is $\theta = k_w z$ (k_w is the wave number for the wiggler period λ_w), which couples to circularly polarized waves that vary as $\exp(i\varphi_h)$, where $\varphi_h = kz + h\theta - \omega t$ is the wave phase. Hence, the phase along the particle trajectories varies as $\varphi_h = (k + hk_w)z - \omega t$, and the hth order azimuthal mode corresponds to the hth harmonic resonance [i.e., $\omega \approx (k + hk_w)v_z$]. Therefore, unlike LHG in planar wigglers, the harmonic interaction in helical wigglers (1) does not depend on the wiggler magnitude and the harmonic growth rates can be comparable to that of the fundamental, and (2) the odd harmonics are not favored. However, these higher order azimuthal modes typically vanish on axis, so that LHG in helical wigglers excites off-axis modes [3] that severely limit harmonic intensities.

In contrast, NHG is driven by nonlinear bunching due to the fundamental and has different properties from LHG. NHG has been studied in planar wigglers in terms of the harmonic bunching [6], three-dimensional nonlinear simulations [7–9], and analytic theory [10] where it has been shown that while the odd harmonics are still preferentially excited the even harmonics are excited as well without recourse to off-axis wiggler components, that the third harmonic can reach intensities of as much as 1% that of the fundamental, and that NHG is much less sensitive to electron beam quality than LHG. It is also important to note that experimental verification of the nonlinear harmonic mechanism has recently been demonstrated in traveling wave tubes [11]. Since FELs and traveling wave tubes share the same axial bunching mechanism, this work provides strong support for NHG in a broad class of electron devices. Note that even harmonic excitation due to NHG is fundamentally different from that for LHG and arises from the nonlinear bunching due to the fundamental. Our conjecture was that on-axis harmonic excitation due to

NHG in helical wigglers can arise because the nonlinear bunching due to the fundamental creates on-axis harmonic source currents which, in turn, excite on-axis harmonic radiation. This conjecture is borne out in simulation.

Thus, NHG has important implications in all classes of FELs. Single-pass FELs operating either by SASE [12,13] or by high-gain harmonic generation [14] are candidates for the next generation x-ray light sources. NHG has been observed, in good agreement with predictions, in both of these cases [15,16]. In these cases, the power achievable by NHG can reduce the beam energy and relax the beam quality needed to reach x-ray wavelengths. In the quest for high average power infrared FEL oscillators [17], NHG can pose difficulties due the potential for mirror damage by harmonic power in the ultraviolet [18]. However, there has been no analysis heretofore of NHG in helical wigglers. Because NHG is driven by the fundamental, which excites on-axis modes, we speculate that NHG in helical wigglers will have substantial on-axis power. To this end, we use the 3D simulation code MEDUSA to describe NHG in helical as well as planar wigglers, and present a comparative analysis of NHG in planar and helical wigglers.

MEDUSA [7] is a three-dimensional, polychromatic simulation code that can model both planar and helical wiggler geometry and treats the electromagnetic field as a superposition of either Gauss-Hermite (planar) or Gauss-Laguerre (helical) modes. The field equations are integrated simultaneously with the three-dimensional Lorentz force equations for an ensemble of electrons. No wiggler-average orbit approximation is used, and MEDUSA can propagate the electron beam through a complex wiggler/transport line including multiple wigglers, quadrupole and dipole magnets, and focusing/defocusing (FODO) lattices.

We use Gauss-Laguerre modes to describe the vector potential of the electromagnetic waves so

$$\delta\mathbf{A}(x,t) = \sum_{l,m,h} e_{l,m,h}(r)[\delta A^{(1)}_{l,m}(z)(\hat{\boldsymbol{e}}_x \sin\varphi_{l,h} \pm \hat{\boldsymbol{e}}_y \cos\varphi_{l,h}) + \delta A^{(2)}_{l,m,h}(z)(\hat{\boldsymbol{e}}_x \cos\varphi_{l,h} \mp \hat{\boldsymbol{e}}_y \sin\varphi_{l,h})], \quad (1)$$

for right- and left-hand circularly polarized waves, where l and m are the radial and azimuthal mode numbers, h is the harmonic number, $\delta A^{(1,2)}_{l,m}(z)$ are the mode amplitudes, $\varphi_{l,h} = h(k_0 z - \omega_0 t) + l\theta + \alpha_h(z) r^2/w_h(z)^2$ is the phase, $k_0 = \omega_0/c$, $e_{l,m,h}(r) = \exp[-r^2/w_h(z)^2]\zeta_h{}^l\ L_m{}^l(\zeta_h^2)$ describes the radial variation of the wave, $\zeta_h \equiv \sqrt{2} r/w_h(z)$, $L_m{}^l(\zeta_h^2)$ is the associated Laguerre polynomial, $w_h(z)$ denotes the radiation spot size, and $\alpha_h(z)$ describes the curvature of the phase front. An adaptive eigenmode algorithm referred to as the source-dependent expansion [19] is used to track the evolution of the mode amplitudes as well as the spot size and curvature self-consistently. The dynamical equations for the fields are

$$\left(\frac{d}{dz} + \frac{w_h'}{w_h}\right)\begin{pmatrix}\delta a^{(1)}_{l,m,h} \\ \delta a^{(2)}_{l,m,h}\end{pmatrix} + K_{l,m,h}\begin{pmatrix}\delta a^{(2)}_{l,m,h} \\ -\delta a^{(1)}_{l,m,h}\end{pmatrix} = \begin{pmatrix}s^{(1)}_{l,m,h} \\ s^{(2)}_{l,m,h}\end{pmatrix}, \quad (2)$$

where $\delta a^{(1,2)}_{l,m,h} = e\delta A^{(1,2)}_{l,m,h}/m_e c^2$ (e is the electronic charge and m_e is the electron rest mass),

$$K_{l,m,h} \equiv (1 + l + 2m)\left[\alpha_h \frac{w_h'}{w_h} - \frac{\alpha_h'}{2} - \frac{1+\alpha_h^2}{k_0 w_h^2}\right], \quad (3)$$

$$\begin{pmatrix}s^{(1)}_{l,m,h} \\ s^{(2)}_{l,m,h}\end{pmatrix} = \frac{\omega_b^2}{k_0 c^2}\frac{m!}{(m+l)!}\frac{w_h(0)^2}{w_h(z)^2} \times \left\langle \frac{e_{l,m,h}}{|v_z|}\begin{pmatrix} v_x\cos\varphi_{l,h} \mp v_y \sin\varphi_{l,h} \\ -v_x \sin\varphi_{l,h} \pm v_y \cos\varphi_{l,h}\end{pmatrix}\right\rangle, \quad (4)$$

and ω_b denotes the beam plasma frequency, and

$$\langle(\cdots)\rangle \equiv \int_0^{2\pi}\frac{d\psi_0}{2\pi}\int_0^\infty d\gamma_0 \frac{\exp[-(\gamma-\overline{\gamma}_0)^2/2\Delta\gamma^2]}{\sqrt{\pi/2}\Delta\gamma[1+\mathrm{erf}(\overline{\gamma}_0/\sqrt{2}\Delta\gamma)]} \times \iiiint dx_0 dy_0 dp_{x0} dp_{y0} \times \frac{\exp(-r_0^2/2\sigma_r^2 - p_{\perp 0}^2/2\sigma_p^2)}{(2\pi)^2\sigma_r^2\sigma_p^2}(\cdots). \quad (5)$$

The spot size and radius of curvature for each harmonic component are governed by

$$w_h' = \frac{2\alpha_h}{hk_0 w_h} - w_h Y_h, \quad (6)$$

$$\frac{\alpha_h'}{2} = \frac{1+\alpha_h^2}{hk_0 w_h^2} - (X_h + \alpha_h Y_h), \quad (7)$$

where the prime superscript denotes a derivative with respect to z,

$$X_h = \frac{s^{(2)}_{0,1,h}\delta a^{(1)}_{0,0,h} - s^{(1)}_{0,1,h}\delta a^{(2)}_{0,0,h}}{\delta a^{(1)2}_{0,0,h} + \delta a^{(2)2}_{0,0,h}}, \quad (8)$$

$$Y_h = \frac{s^{(1)}_{0,1,h}\delta a^{(1)}_{0,0,h} + s^{(2)}_{0,1,h}\delta a^{(2)}_{0,0,h}}{\delta a^{(1)2}_{0,0,h} + \delta a^{(2)2}_{0,0,h}}. \quad (9)$$

In the absence of the beam $X_h = Y_h = 0$, Eqs. (6) and (7) recover vacuum diffraction where $w_h = w_h(z=0)\times[1 + z^2/z_{0h}^2]^{1/2}$, $\alpha_h = z/z_{0h}$, and $z_{0h} = hk_0 w_h{}^2(z=0)/2$ is the Rayleigh range.

We now consider an infrared FEL oscillator operating at a wavelength near 1 micron. The electron beam is characterized by a 140 MeV energy, an 800 A peak current, and a normalized emittance of 1.9 mm mrad. We consider energy spreads up to 0.9%. The on-axis (helical) wiggler amplitude is 7.14 kG and the period is 3.0 cm. The optimal fundamental resonance is at 1.04 microns. The electron beam is matched to the beta function in the wiggler, and the radius is about 110 microns. The resonator mode is focused to a waist at the center of the wiggler, which must be comparable to the beam radius for a strong interaction. For such a small electron beam, this implies that the Rayleigh range is short. Because the interaction strength decreases rapidly as the mode expands, the wiggler must be short as well. We assume that the waist is 80 microns, for a Rayleigh range of 3.867 cm. The wiggler length is assumed

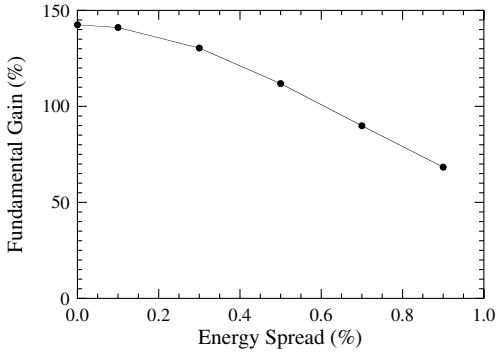

FIG. 1. Variation in the single-pass gain at the fundamental with beam energy spread.

to be 0.78 m with three wiggler period transitions at both ends and a uniform field region of 20 wiggler periods.

Since MEDUSA is in the frequency domain, it treats oscillators in the steady-state regime. In this process, we study the single-pass gain as a function of initial (drive) power. As the oscillator drive power enters the nonlinear regime, the single-pass gain drops and saturation occurs when the gain falls to the level of resonator losses including the out-coupled power and losses in the mirrors.

The variation in the small-signal (i.e., linear) single-pass gain at the fundamental for this oscillator with energy spread is shown in Fig. 1. Despite the short wiggler and Rayleigh range, the optimal single-pass gain at low beam energy spread is still about 140%, but the gain drops rapidly to about 68% as the energy spread increases to 0.9%.

A drive curve showing the variation of the single-pass gain at the fundamental (circles and the left axis) and the harmonic powers (right axis) versus fundamental input power for an energy spread of 0.1% is shown in Fig. 2. As mentioned, saturation occurs when the fundamental gain falls to the level of the resonator losses; hence, this figure may be interpreted as follows. For a given resonator loss rate, the gain curve yields the saturated power by finding the input power corresponding to the loss rate. If the loss rate is 50%, then the saturated fundamental peak power for this energy spread is about 2 GW. The harmonic powers associated with this saturation point correspond to

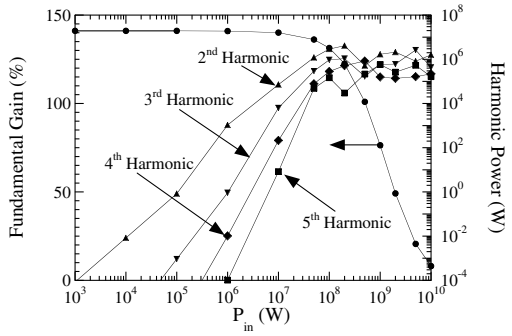

FIG. 2. Drive curves showing the single-pass gain (fundamental) and the second through fifth harmonic powers versus the fundamental drive power for a 0.1% energy spread.

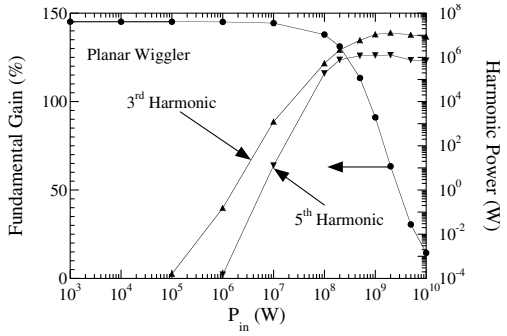

FIG. 3. Drive curves showing the single-pass gain (fundamental) and the third and fifth harmonic powers versus the fundamental drive power in a planar wiggler for a 0.1% energy spread.

a 2 GW input power, and the power at the second harmonic is 2.12 MW, at the third harmonic it is 610 kW, at the fourth harmonic it is 138 kW, and at the fifth harmonic it is 537 kW. Since these are peak powers, knowledge of the duty factor is necessary to determine the average power.

Several characteristics of the NHG should be noted. First, the harmonic power prior to saturation varies as the fundamental drive power to the hth power (i.e., $P_{in}{}^{h}$), as in planar wiggler oscillators [18]. Second, the harmonics saturate shortly after the fundamental enters the nonlinear regime and oscillates thereafter. Third, while the first peaks in the harmonic powers decrease, albeit slowly, with increasing harmonic number, the oscillations in the powers after the initial peak show a weaker dependence on harmonic number. Here, the second through fifth harmonics are in the range 10^5–10^6 W, and substantial powers can be expected at still higher harmonics. This weak dependence of NHG on harmonic number is similar to the previously described nature of LHG in helical wigglers [3], and arises from the nature of the azimuthal resonance condition.

It is useful to compare NHG in helical and planar wigglers, and we show the fundamental gain and harmonic powers versus initial fundamental drive power for a planar wiggler in Fig. 3 for parameters identical to those in Fig. 2, except that the on-axis wiggler field is increased to 10.06 kG. In addition, we only show the third and fifth harmonics because the even harmonics have much lower

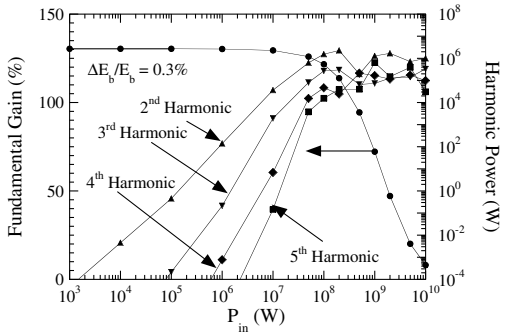

FIG. 4. Drive curves showing the single-pass gain (fundamental) and the second through fifth harmonic powers versus the fundamental drive power for a 0.3% energy spread.

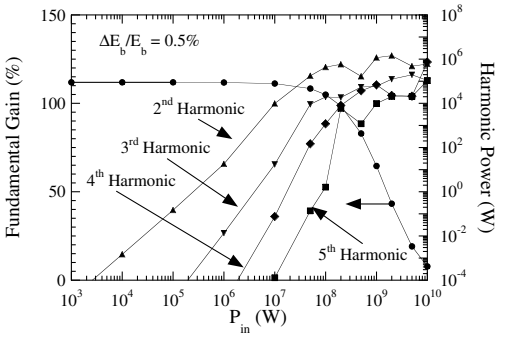

FIG. 5. Drive curves showing the single-pass gain (fundamental) and the second through fifth harmonic powers versus the fundamental drive power for a 0.5% energy spread.

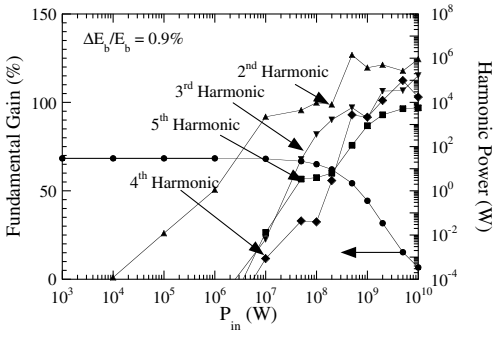

FIG. 6. Drive curves showing the single-pass gain (fundamental) and the second through fifth harmonic powers versus the fundamental drive power for a 0.9% energy spread.

powers. The third (fifth) harmonic power reaches a maximum of about 13 MW (1.3 MW) and varies slowly with drive power after the maximum. This contrasts with the more rapid oscillations in harmonic power after the first peak found in the helical wiggler. In addition, the powers in the third harmonic in the planar wiggler exceed those found in the helical wiggler, and the fifth harmonic is comparable to that found in the second harmonic for the helical wiggler. Thus, the first two odd harmonics in the planar wiggler have comparable or higher powers than found in the helical wiggler. However, because of the more gradual decline in harmonic power with harmonic number in helical wigglers, we expect that still higher harmonics may have higher powers in helical than in planar wigglers.

It has been shown that NHG in planar wigglers is relatively insensitive to energy spread [9], and this is also found in helical wigglers. This is illustrated in Figs. 4–6 where we plot the fundamental gain (left axis) and harmonic powers (right axis) versus fundamental drive power for energy spreads of 0.3%, 0.5%, and 0.9%, respectively. The peak second harmonic power shown in Fig. 4 experiences a negligible decline with respect to the case of a 0.1% energy spread, and the higher harmonic powers still fall within the range of 10^5–10^6 W. For an energy spread of 0.5% (Fig. 5), the peak second harmonic power drops further but is still of the order of 1 MW. The higher harmonic powers also decline but are still in the range of 10^4–10^5 W. For an energy spread of 0.9% (Fig. 6), we see further declines in the harmonic powers but the second harmonic still reaches MW power levels and the higher harmonics still fall within the range of 10^4–10^5 W. The ambiguity in the harmonic powers arises because the specific power levels depend upon the resonator losses that are largely determined by output coupling.

In summary, we have presented the formulation for the three-dimensional simulation of helical wiggler FELs including harmonic generation and applied the analysis to the study of NHG in FEL oscillators. The analysis shows that NHG in helical wigglers is strong and, in contrast to planar wigglers, excites even and odd harmonics at comparable power levels. For the specific parameters studied, the powers reached by the third and fifth harmonics in a planar wiggler are comparable to or exceed that found for the harmonics in the helical wiggler; however, the decline in harmonic power is more gradual in helical wigglers so that the harmonic powers at still higher harmonics may exceed that found in planar wigglers. Finally, as previously demonstrated for planar wigglers [9], NHG in helical wigglers is relatively insensitive to energy spread.

This work was supported by the Office of Naval Research, the Joint Technology Office, and the U.S. Department of Energy under Contract No. W-31-109-ENG-38.

[1] B. M. Kincaid, J. Appl. Phys. **48**, 2684 (1977).
[2] L. R. Elias, Phys. Rev. Lett. **36**, 717 (1976).
[3] H. P. Freund and T. M. Antonsen, Jr., *Principles of Free-Electron Lasers* (Chapman and Hall, London, 1996), Chap. 7.
[4] W. B. Colson, IEEE J. Quantum Electron. **QE-17**, 1417 (1981).
[5] M. J. Schmitt and C. J. Elliot, Phys. Rev. A **34**, 4843 (1986).
[6] R. Bonifacio *et al.*, Nucl. Instrum. Methods Phys. Res., Sect. A **293**, 627 (1990).
[7] H. P. Freund *et al.*, IEEE J. Quantum Electron. **36**, 275 (2000).
[8] H. P. Freund *et al.*, IEEE J. Quantum Electron. **37**, 790 (2001).
[9] S. G. Biedron *et al.*, Phys. Rev. ST Accel. Beams **5**, 030701 (2002).
[10] Z. Huang and K. J. Kim, Phys. Rev. E **62**, 7295 (2000).
[11] A. Singh *et al.*, Phys. Rev. Lett. **92**, 205005 (2004).
[12] LCLS Design Group, LCLS Design Report, NTIS Doc. No. DE98059292, 1998.
[13] J. Rossbach, Nucl. Instrum. Methods Phys. Res., Sect. A **375**, 269 (1996).
[14] L. H. Yu *et al.*, Science **289**, 932 (2000).
[15] S. G. Biedron *et al.*, Nucl. Instrum. Methods Phys. Res., Sect. A **483**, 94 (2002).
[16] A. Doyuran *et al.*, Nucl. Instrum. Methods Phys. Res., Sect. A **475**, 260 (2001).
[17] G. R. Neil *et al.*, Phys. Rev. Lett. **84**, 662 (2000).
[18] H. P. Freund *et al.*, Nucl. Instrum. Methods Phys. Res., Sect. A **528**, 44 (2004).
[19] P. Sprangle *et al.*, Phys. Rev. A **36**, 2773 (1987).